

# A quantum network of clocks

P. Kómár,<sup>1,\*</sup> E. M. Kessler,<sup>1,2,\*</sup> M. Bishof,<sup>3</sup> L. Jiang,<sup>4</sup> A. S. Sørensen,<sup>5</sup> J. Ye,<sup>3</sup> and M. D. Lukin<sup>1</sup>

<sup>1</sup>*Physics Department, Harvard University, Cambridge, Massachusetts 02138, USA*

<sup>2</sup>*ITAMP, Harvard-Smithsonian Center for Astrophysics, Cambridge, MA 02138, USA*

<sup>3</sup>*JILA, NIST, Department of Physics, University of Colorado, Boulder, CO 80309, USA*

<sup>4</sup>*Department of Applied Physics, Yale University New Haven, CT 06520, USA*

<sup>5</sup>*QUANTOP, Danish National Research Foundation Centre of Quantum Optics,*

*Niels Bohr Institute, DK-2100 Copenhagen, Denmark*

(Dated: October 24, 2013)

The development of precise atomic clocks has led to many scientific and technological advances that play an increasingly important role in modern society. Shared timing information constitutes a key resource for positioning and navigation with a direct correspondence between timing accuracy and precision in applications such as the Global Positioning System (GPS). By combining precision metrology and quantum networks, we propose here a quantum, cooperative protocol for the operation of a network consisting of geographically remote optical atomic clocks. Using non-local entangled states, we demonstrate an optimal utilization of the global network resources, and show that such a network can be operated near the fundamental limit set by quantum theory yielding an ultra-precise clock signal. Furthermore, the internal structure of the network, combined with basic techniques from quantum communication, guarantees security both from internal and external threats. Realization of such a global quantum network of clocks may allow construction of a real-time single international time scale (world clock) with unprecedented stability and accuracy.

With the advances of highly phase coherent lasers, optical atomic clocks containing multiple atoms have demonstrated stability that reaches the standard quantum limit (SQL) set by the available atom number within a clock [1, 2]. Reaching beyond SQL, we stand to gain a significant improvement of clock performance by preparing atoms in quantum correlated states (e.g., spin squeezed states [3]). Here we describe a new approach to maximize the performance of a network composed of multiple clocks allowing to gain advantage of all resources available at each node. Several recent advances in precision metrology and quantum science make this approach realistic. On the one hand, capabilities to maintain phase coherent optical links spanning the entire visible spectrum and over macroscopic distances have been demonstrated, with the capability of delivering the most stable optical oscillator from one color or location to another [4, 5]. On the other hand, quantum communications and

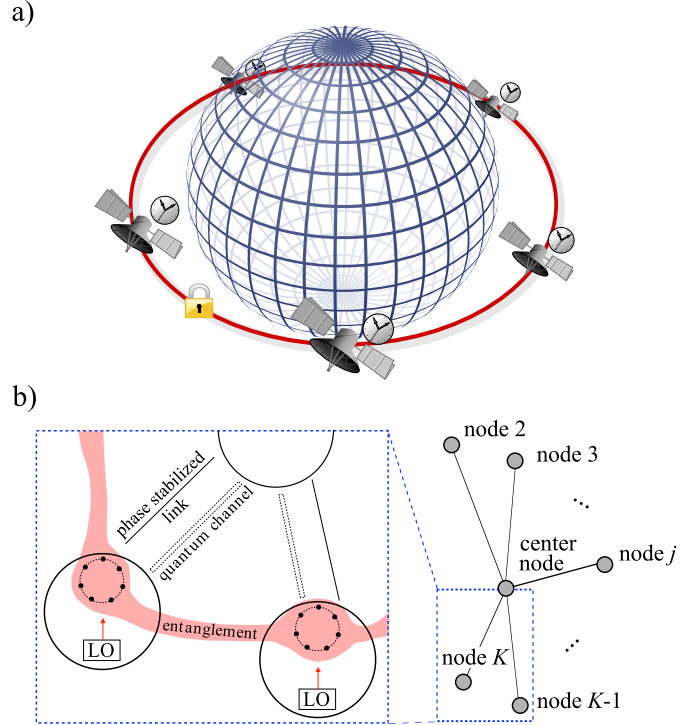


FIG. 1. The concept of world-wide quantum clock network. a) Illustration of a cooperative clock operation protocol in which individual parties (e.g., satellite based atomic clocks from different countries) jointly allocate their respective resources in a global network involving entangled quantum states. This guarantees an optimal use of the global resources, achieving an ultra-precise clock signal limited only by the fundamental bounds of quantum metrology and, in addition, guaranteeing secure distribution of the clock signal. b) In addition to locally operating the individual clocks, the different nodes (i.e., satellites) employ network-wide entangled states to interrogate their respective local oscillators (LOs). The acquired information is sent to a particular node serving as a center where it is used to stabilize a center of mass mode of the different LOs. This yields an ultra-precise clock signal accessible to all network members.

entanglement techniques are enabling distant quantum objects to be connected in a quantum network [6–8], that can enable novel, extraordinary capabilities. Combining these two technological frontiers, we show here that a distributed network composed of quantum-limited clocks

\* These authors contributed equally to this work

separated by large distances – as appropriate, e.g., for the satellite-based clocks possibly operated by different nations – can be operated as an ultimate “world clock”, where all members combine their individual resources in a quantum coherent way to achieve greater clock stability and distribute this international time scale in real time for all.

The distributed architecture allows each participant of the network to profit from a stability of the local clock signal that is enhanced by a factor proportional to the total number of parties (as compared to an independent operation of the individual clocks) without losing sovereignty or compromising security. This cooperative gain strongly incentivizes joining the collaborative network while retaining robustness against disruptions of communication channels by allowing the parties to fall back to individual clock operation. Our scheme is superior to an alternative approach of disseminating the time signal from a single location containing all qubits, since errors arising from imperfect phase links can be largely reduced by relying on the stabilized and locally available local oscillators. We demonstrate that by preparing quantum-correlated states of remote clocks, the network can yield the best possible clock signal allowed by quantum theory for the combined resources. Furthermore, enabled through the use of quantum communication techniques, such a network can be made secure, such that only parties contributing to its operation may enjoy the benefit of an ultra-precise clock signal. Besides serving as a real-time clock for the international time scale, the proposed quantum network also represents a large-scale quantum sensor that can be used to probe the fundamental laws of physics, including relativity and connections between space-time and quantum physics.

## THE CONCEPT OF QUANTUM CLOCK NETWORK

Fig. 1 illustrates the basic concept for the proposed quantum clock network. We consider a set of  $K$  atomic clocks (constituting the nodes of the network), each based on a large number of atoms (clock qubits) serving as the frequency reference  $\omega_0$  at different geographical locations. In our approach, each clock has its own independently operated local oscillator (LO),  $\mathcal{E}_j(t) \propto e^{i\nu_j t}$ , with detuning  $\delta_j = \nu_j - \omega_0$ , ( $j = 1, 2 \dots K$ ). It keeps the time by interrogating its qubits periodically, and uses the measurement data to stabilize the LO frequency at the reference frequency of the atomic transition. However, as opposed to the conventional approach, in which each LO interrogates its own independent qubits, we consider the situation in which each network node allocates some of its qubits to form entangled states stretching across all nodes. When interrogated within a properly designed measurement scheme, such entangled network states provide ultra-precise information about the deviation of the center-of-mass (COM) frequency  $\nu_{\text{COM}} = \sum_j \nu_j / K$  of all

local oscillators from the atomic resonance.

Each clock cycle consists from three stages: preparation of the clock atom state (initialization), interrogation by the LOs (measurement) and correction of the laser frequency according to the measurement outcome (feedback). In the further analysis, we assume, for convenience, that in each interrogation cycle one of the nodes plays the role of an alternating center, which initiates each Ramsey cycle and collects the measurement data from the other nodes via classical channels [Fig. 1 b)], as well as LO signals via optical links, to feedback the COM signal. (In practice, it is straightforward to devise a similar network with same functionality and a flat hierarchical structure where no center is needed, see Supplementary Information). This information, in turn, can be utilized in a feedback cycle to yield a Heisenberg-limited stability of the COM clock signal generated by the network, which is subsequently distributed to the individual nodes in a secure fashion. As a result, after a few cycles, the LOs corresponding to each individual node achieve an accuracy and stability effectively resulting from interrogating atoms in the entire network.

## PREPARATION OF NETWORK-WIDE ENTANGLED STATES

In the initialization stage of each clock cycle, entangled states spanning across the nodes at different geographical positions of the network are prepared. In the following, we describe exemplarily how a single network-wide GHZ state can be prepared. The entangled states employed in the proposed quantum network protocol – which are described in the following section – consist of products of GHZ states of different size. They can be prepared by repetition of the protocol that we now describe.

For simplicity, we assume that each node  $j$  ( $j = 1, \dots, K$ ) contains an identical number  $n$  of clock qubits which we label as  $1_j, 2_j, \dots, n_j$  (in the Supplementary Information we discuss the case where the nodes contain different amounts of clock qubits). Further, we assume, for convenience, that the center node ( $j = 1$ ) has access to additional  $2(K - 1)$  ancilla qubits  $a_2, \dots, a_K, b_2, \dots, b_K$  besides the  $n$  clock atoms (a slightly more complicated procedure allows to refrain from the use of ancilla qubits, see Supplementary Information). The entangling procedure starts at the center with the creation of a fully entangled state of one half of the ancilla qubits  $\{b_j\}$ , and its first clock qubit  $1_1$ . This can be realized, e.g. with a single qubit  $\pi/2$ -rotation (on qubit  $1_1$ ) and a series of controlled not (CNOT) gates [9] (between  $1_1$  and each  $b_j$ ). The result is a GHZ state,  $[|00 \dots 0\rangle_{1_1, b_2, b_3, \dots, b_K} + i|11 \dots 1\rangle_{1_1, b_2, b_3, \dots, b_K}] / \sqrt{2}$ . In parallel, the center uses the other half of the ancillas  $\{a_j\}$  to create single EPR pairs with each node  $j \neq 1$ , either by directly sending flying qubits and converting them to stationary qubits, or by using quantum repeater techniques to prepare high-fidelity entanglement [10]. As a

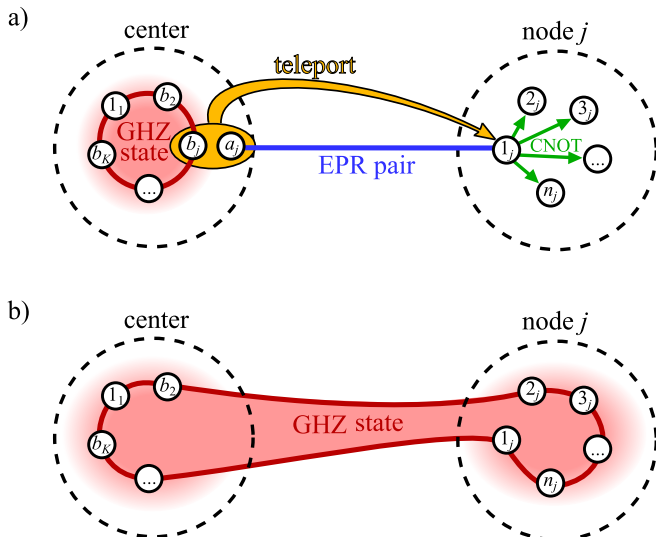


FIG. 2. Entangled state preparation between distant nodes. a) The center node ( $j = 1$ ) initiates the initialization sequence by preparing a local GHZ state across the qubits  $\{b_j\}_{j=2}^K$  and  $1_1$ , as well as  $(K - 1)$  EPR pairs on the qubit pairs  $\{(a_j, 1_j)\}_{j=2}^K$ . Quantum teleportation expands this GHZ state to the first qubit within each of the individual nodes. b) Originating from the teleported qubits, the nodes grow the GHZ state to involve all the desired local qubits by employing local entangling operations. The procedure results in a common GHZ states over all atoms of the nodes.

result of this procedure, one part of the pair is stored at the center node (qubit  $a_j$ ), while the other one is stored at the  $j$ th node (qubit  $1_j$ ), forming the states  $[|00\rangle_{a_j, 1_j} + |11\rangle_{a_j, 1_j}]/\sqrt{2}$  for every  $j$  (see Fig. 2).

Next, the center performs  $K - 1$  separate Bell measurements on its ancilla qubit pairs  $\{(b_j, a_j)\}$ . This teleports the state of qubit  $b_j$  to qubit  $1_j$  ( $j = 2, \dots, K$ ), up to a local single-qubit rotation, which is performed after the measurement outcomes are sent to the node via classical channels. The result of the teleportations is a collective GHZ state  $\frac{1}{\sqrt{2}}|00\dots 0\rangle_{1_1, 1_2, \dots, 1_K} + i|11\dots 1\rangle_{1_1, 1_2, \dots, 1_K}$ , stretching across the first qubits of all  $K$  nodes.

In the final step of entangling, all nodes (including the center) extend the entanglement to all of their remaining clock qubits. To do this, each node  $j$  performs a series of CNOT gates controlled on  $1_j$  and targeting qubits  $2_j, 3_j, \dots, n_j$ . At the end of the protocol the different nodes share a common GHZ state  $[|\mathbf{0}\rangle + i|\mathbf{1}\rangle]/\sqrt{2}$ , where  $|\mathbf{0}\rangle$  and  $|\mathbf{1}\rangle$  are product states of all qubits  $\{i_j : i = 1, 2, \dots, n, j = 1, 2, \dots, K\}$  being in  $|0\rangle$  or  $|1\rangle$ , respectively. As discussed below, in practice the entanglement distribution can be done either via polarization- or frequency-entangled photons with frequency difference in the microwave domain, in which case the ancillary qubits involved in the entanglement distribution will be different from the clock qubits. Typically, as part of the preparation process, time delays arise between the initialization of different clock qubits. Its detrimental effects can be

entirely avoided by proper local timing or prior preparation of entanglement, as discussed in the Supplementary Information.

## INTERROGATION

The use of entangled resources (in form of network-wide GHZ-like states) during the interrogation phase enables an optimal use of the available resources via the following procedure. Assume we have a total of  $\tilde{N}$  qubits at our disposal which are equally distributed between the  $K$  nodes (indexed  $j = 1, \dots, K$ ) and prepared in a non-local GHZ state  $[|\mathbf{0}\rangle + i|\mathbf{1}\rangle]/\sqrt{2}$ , where  $|\mathbf{0}(\mathbf{1})\rangle \equiv |0(1)\rangle^{\otimes \tilde{N}}$ . During the interrogation time  $T$ , a clock qubit at node  $j$  picks up a relative phase  $\phi_j = \delta_j T$ . Due to the non-local character of the state, these phases accumulate in the total state of the atoms  $[|\mathbf{0}\rangle + ie^{i\Phi}|\mathbf{1}\rangle]/\sqrt{2}$ , where the collective phase after the interrogation time  $T$  is given as

$$\Phi = \sum_{j=1}^K \frac{\tilde{N}}{K} \phi_j = \tilde{N} \delta_{\text{COM}} T, \quad (1)$$

where  $\delta_{\text{COM}} = \nu_{\text{COM}} - \omega_0$ . To extract the phase information picked up by the different GHZ states, after each interrogation phase, the individual nodes  $j$  measure their respective qubits in the  $x$ -basis, and evaluate the parity of all measurement outcomes  $p_j$ . Subsequently, the nodes send this information to the center node via a classical channel, where the total parity  $p = \prod_j p_j$  is evaluated, and the phase information is extracted [14, 15]. Note, that only the full set  $\{p_j | j = 1 \dots K\}$  contains information. This can be interpreted as only the center node holding the key, namely its own measurement outcome  $p_1$ , to decode the phase information sent from the nodes.

The proportionality with  $\tilde{N}$  in Eq. (1) represents the quantum enhancement in the estimation of  $\delta_{\text{COM}}$ . However, for realistic laser noise spectra, this suggested enhancement is corrupted by the increase of uncontrolled phase slips for a single GHZ state [11]: Whenever after the Ramsey time the phase  $\Phi$  – which due to the laser frequency fluctuations constitutes a random variable itself – falls out of the interval  $[-\pi, \pi]$  the estimation fails. This limitation restricts the maximal Ramsey time to values  $T < (\tilde{N} \gamma_{\text{LO}})^{-1}$ , preventing any quantum gain in the estimation.

To circumvent this problem, we use entangled states consisting of products of successively larger GHZ ensembles, see SI and [12]. In this approach, interrogated network atoms are split into several independent, shared groups. We write the number of the first group of atoms as  $\tilde{N} = 2^{M-1}K$ , for some natural number  $M$ . Furthermore, the network shares additional groups of atoms, each containing  $2^i K$  ( $i = 0, \dots, M - 2$ ) equally distributed between the nodes and prepared in GHZ states. Finally, each node has a small number of uncorrelated atoms interrogated by LOs. Using a protocol reminiscent of the phase estimation algorithm [9, 12, 13]

these states allow to directly assess the bits  $Z_i \in \{0, 1\}$  of the binary fraction representation of the laser phase  $\Phi_{\text{LO}} = \delta_{\text{COM}} T = 2\pi[(Z_1 - 1)2^{-1} + Z_2 2^{-2} + Z_3 2^{-3} \dots]$ . This yields an estimate of  $\Phi_{\text{LO}}$  with Heisenberg-limited accuracy, up to a logarithmic correction, see SI:

$$\Delta\Phi_{\text{LO}} = \frac{8}{\pi} \log(N)/N, \quad (2)$$

even for Ramsey times beyond the limits of the laser frequency fluctuations [ $T > (\tilde{N}\gamma_{\text{LO}}^{-1})$ ], where  $N$  represent the total number of clock atoms employed in the scheme. The logarithmic correction arises due to the number of particles required to realize this (incoherent) version of the phase estimation algorithm.

### FEEDBACK

The measured value of the phase  $\Phi_{\text{LO}}$ , gives an estimate on the COM detuning  $\delta_{\text{COM}}$  after each Ramsey cycle, which is subsequently used by the center node to stabilize the COM laser signal. To this end the center generates the COM of the frequencies. Every node sends its local oscillator field  $\mathcal{E}_i$  to the center via phase-stable optical links, and the center synthesizes the COM frequency  $\nu_{\text{COM}}$  by averaging the  $\nu_j$  frequencies with equal weights [16]. This can be implemented via heterodyne beat of the local oscillator in the center against each incoming laser signal, resulting in  $K$  beat frequencies. Synthesizing these beat frequencies allows the local oscillator of the central node to phase track  $\nu_{\text{COM}}$ . The center distributes the stabilized clock signal to different members of the network by sending individual error signals  $\delta_j = \delta_{\text{COM}} + (\nu_j - \nu_{\text{COM}})$  to all nodes  $j$ , respectively, and corrects its own LO as well, accordingly. Alternatively, the center can be operated to provide restricted feedback information to the nodes, see SI.

### STABILITY ANALYSIS

In this section, we demonstrate that the proposed quantum clock network achieves the best clock signal, allowed by quantum theory for the available resources, i.e. the total atom number. Rather than individually operating their respective LOs the joint use of resources allows the network to directly interrogate and stabilize the COM mode of the lasers. To quantify this cooperative gain, we compare networks of different types (classical or quantum mechanical interrogation of the respective LOs) and degrees of cooperation (no cooperation, classical, or quantum cooperation).

First, we analyze the stability of the proposed quantum clock network, corresponding to the case of quantum interrogation and cooperation (curve a in Fig. 3). In this case, the analysis resulting in Eq. (2) suggests that near Heisenberg-limited scaling with a total atom number can

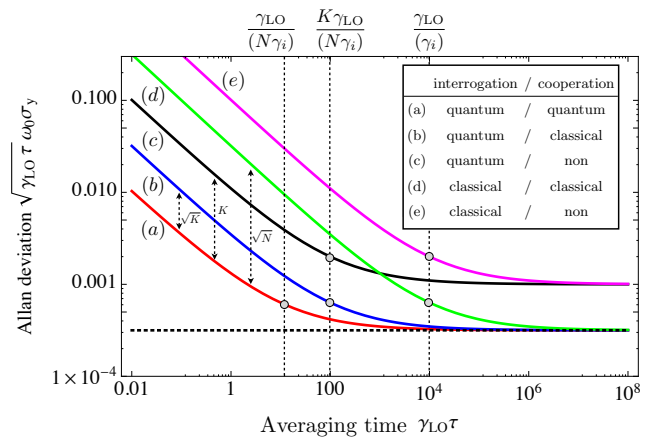


FIG. 3. Performance of different operation schemes. Comparison of the achievable (rescaled) Allan deviation  $\sqrt{\gamma_{\text{LO}} \tau \omega_0 \sigma_y}$  using clock networks of different types and degrees of cooperation. (a) the proposed protocol realizing quantum interrogation and cooperation, (b) quantum interrogation and classical cooperation, (c) quantum interrogation and no cooperation, (d) classical interrogation and classical cooperation, (e) classical interrogation and no cooperation (cf. text). The dotted base line represents the fundamental bound arising from the finite width of the clock atoms transition [compare Eq. (4)]. This optimal stability can be attained only via cooperation between the nodes. The quantum clock network (a) represents the optimal form of cooperation, and reaches this boundary faster than any other operational mode. Parameters are  $N = 1000$ ,  $K = 10$ ,  $\gamma_i = 10^{-4} \gamma_{\text{LO}}$ .

be achieved for the entangled clock network. In particular, for a given total particle number  $N$  and for averaging times shorter than the timescale set by individual qubit noise  $\tau < 1/(\gamma_i N)$  (where  $\gamma_i$  is the atomic linewidth), the network operation achieves a Heisenberg-limited Allan deviation (ADEV) of the COM laser mode

$$\sigma_y(\tau) = \frac{1}{\omega_0 \sqrt{n_0} 2^M K} \frac{1}{\tau} \sim \frac{\sqrt{\log(N)}}{\omega_0 N} \frac{1}{\tau}, \quad (3)$$

up to small numerical corrections. Here, the number of GHZ copies per group  $n_0 \sim \log(N)$  ( $N \approx n_0 2^{M+1} K$ ) is found after optimization [cf. SI], and gives rise to a logarithmic correction in the total particle number. The  $1/\tau$  scaling results from the effective cancellation of the low frequency part of the laser noise spectrum, achieved by the cascaded protocol described above, possibly in combination with additional stages of uncorrelated interrogations using varying Ramsey times [17, 18], see [12]. This allows the cycle time  $T$  (which is assumed to be equal to the interrogation time) to be extended to the total available measurement time  $\tau$ .

Eventually, for large averaging times  $\tau > 1/(\gamma_i N)$  the Ramsey time becomes fundamentally limited by individual noise processes ( $T \leq 1/(\gamma_i N)$ ). As a result, the  $1/N$  scaling breaks down, and the ADEV returns to the square root scaling with both the employed particle number and

averaging time,

$$\sigma_y(\tau) \sim \frac{1}{\omega_0 \sqrt{N}} \sqrt{\frac{\gamma_i}{\tau}}, \quad (4)$$

up to constant numerical factors. Eq. (4) results from fundamental quantum metrological bounds [19], and represents the best conceivable clock stability in the presence of individual particle decoherence which, in a network, can only be achieved via cooperation. Independently operating a clock, in contrast, can only achieve a stability scaling with the local number of atoms, i.e.  $\sigma_y(\tau) \propto \sqrt{K/N}$ .

Fig. 3 illustrates the comparison of entangled clock network with other approaches. A network in which the  $K$  nodes cooperate classically (curve b in Fig. 3), by locally measuring the individual phase deviation  $\phi_j$ , and combining the outcomes via classical channels, outperforms individually operated clocks (curve c) by a factor of  $\sqrt{K}$  (for both cases, assuming optimal quantum interrogation for individual nodes [12, 20]). The quantum network protocol (curve a) increases this cooperative advantage by an additional factor of  $\sqrt{K}$  for short averaging times, reaching Heisenberg-limit. The ADEV converges to the fundamental bound [Eq. (4)]  $K$  times faster compared to the case of classical cooperation (curve b). Although an optimal, classical, local protocol (e.g. [17, 18]), combined with classical cooperation (curve d), eventually reaches the same bound [Eq. (4)], this approach is atom-shot noise limited, and hence its stability is reduced by a factor of  $\sqrt{N}$  for short averaging times [compare Eq. (3)] compared to the quantum network protocol. Hence, the optimal stability [Eq. (4)] is reached at averaging times that are  $N$  times longer than for the proposed quantum network. Naturally, all of the above approaches are superior to a classical scheme without cooperation (curve e).

As a specific example, we first consider ion clocks that can currently achieve a stability of  $2.8 \times 10^{-15}$  after 1 s of averaging time [22]. The entangled states of up to 14 ions has already been demonstrated [24] as was the entanglement of remote ions [40]. We consider a network of ten clocks, each containing ten ions. Using  $\text{Al}^+$  ( $\omega_0 = 2\pi \times 1121$  THz,  $\gamma_i = 2\pi \times 8$  mHz), we find that the quantum cooperative protocol can reach  $4 \times 10^{-17}$  fractional frequency uncertainty after 1 s. Even more pronounced improvement could potentially be achieved using e.g.  $\text{Yb}^+$  ions, due to the long coherence time ( $2.2 \times 10^4$  s) of its octupole clock transition.

The quantum gain could be even more pronounced for neutral atomic clocks. For a network consisting of ten clocks similar to the one operated in JILA [1], each containing 1000 neutral atoms with central frequency  $\omega_0 = 2\pi \times 429$  THz and linewidth  $\gamma_i = 2\pi \times 1$  mHz, the quantum cooperative scheme can achieve a stability of  $\sim 2 \times 10^{-18}$  after 1s averaging, and is an order of magnitude better than the best classical cooperative scheme. Future advances, allowing to employ clock transitions with linewidths of a few tens of  $\mu\text{Hz}$  (such as

erbium), could possibly allow for further improvement, achieving fractional frequency uncertainty beyond  $10^{-20}$  after  $\tau \sim 100$  s. This level of stability is in the same order of magnitude then the required sensitivity to successfully use the network as a gravitational interferometer [44].

## SECURITY

A network with such precise time-keeping capabilities can be subject to both internal and external attacks. Effectively countering them is crucial to establish a reliable ground for cooperation. We consider the network secure if the implemented countermeasures can prevent external parties from benefiting from the network (eavesdropping), as well as effectively detect any malicious activities of any of the members (sabotage).

Sabotage describes the situation where one of the nodes – intended or unintended – operates in a damaging manner. For example, one node could try sending false LO frequencies or wrong measurement bits in the hope of corrupting the collective measurement outcomes. In order to detect such malicious participants, the central node can occasionally perform assessment tests of the different nodes by teleporting an uncorrelated qubit state  $[|0\rangle + e^{i\chi}|1\rangle]/\sqrt{2}$ , where  $\chi$  is a randomly chosen phase known only to the center. By checking for statistical discrepancies between the measurement results and the detuning of the LO signal sent by the node under scrutiny, the center can rapidly and reliably determine whether the particular node is operating properly (See Fig. 4a and Supplementary Information).

Eavesdropping, i.e., the unauthorized attempt to access the stabilized  $\nu_{\text{COM}}$  frequency, can be prevented by encoding the classical channels, over which the center and the nodes exchange feedback signals, using quantum key distribution protocols [21]. Our protocol can keep the stabilized signal hidden from outsiders by mixing the feedback signal with the LO signal at each node only after the non-stabilized LO has been sent to the center (see Fig. 4b and SI). As a result, even if all LO signals are intercepted, the eavesdropper is able to access only the non-stabilized COM signal. Furthermore, the center exclusively can decode the measurement results sent by the individual nodes using its own measurement outcomes as mentioned above. As a result, the stabilized COM signal remains accessible exclusively to parties involved in the collaboration.

Finally, we note that a distributed operation offers significant security advantages over an alternative approach of having all resources combined in one place from where the signal is distributed. In case of a physical attack of the network, disabling the center or the communication links, the nodes can fall back to an independent clock operation using their local resources.

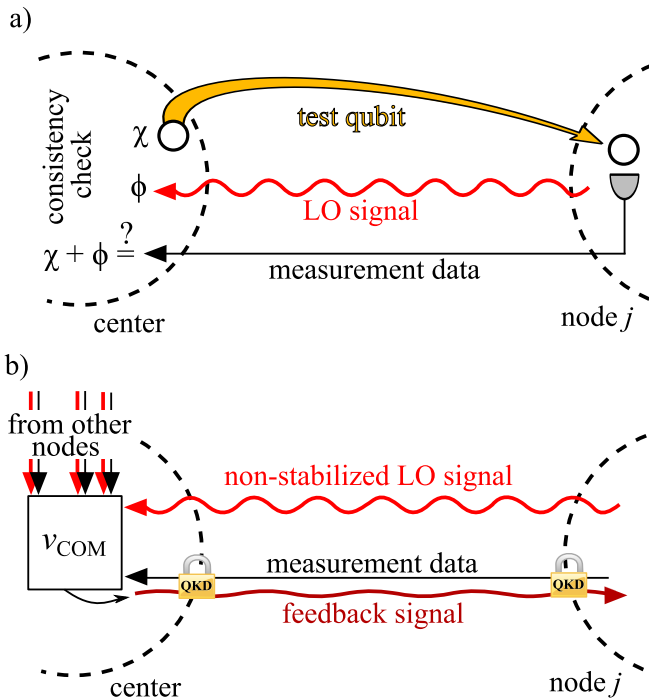


FIG. 4. Schematics of security countermeasures. a) The center node can choose to test any node  $j$  by teleporting a disentangled qubit with a certain phase rotation. A properly operating node creates a local GHZ state  $[|0\rangle + e^{i\chi}|1\rangle]/\sqrt{2}$  from the sent qubit, measures the parity of the GHZ state, and sends it to the center. The measured parity holds information on the phase  $\phi' = \chi + \phi$ , where  $\phi$  is the accumulated phase of the LO at the node. The center verifies  $\phi$  by comparing it with the classically determined phase of the sent LO signal with respect to the COM signal. b) Eavesdropping can be prevented by prescribing that only the non-stabilized LO signals are sent through classical channels and encoding the radio frequency feedback signal with phase modulation according to a shared secret key.

## OUTLOOK

One of the advantages of the proposed quantum clock network involves its ability to maintain and synchronize the time standards across multiple parties in the real-time. Unlike the current world time standard, where the individual signals from different clocks are averaged and communicated with a time delay (a so called paper clock), in our quantum clock network all participants have access to the ultra-stable signal at any time. Furthermore, by having full access to their local clocks the different parties keep their full sovereignty and ensure security, as opposed to a joint operation of a single clock.

Realization of the full-scale network of the type described here will require a number of technological advances in both metrology and experimental quantum information science. The remote entanglement can be implemented by using recently demonstrated techniques for individual atom-photon entanglement [25–29]. Since the teleportation protocol requires quantum links capable of

sharing EPR pairs with sufficiently high repetition rate and fidelity, entanglement purification [30] and quantum repeater techniques [10] will likely be required. In practice, qubits used for entanglement distribution may not be ideal for clocks. However, as noted previously remote entanglement does not need to involve coherent qubits at optical frequencies (e.g., polarization entanglement can be used). In such a case, the use of hybrid approaches, combining different systems for entanglement and local clock operations, may be warranted. It might also be interesting to explore if high-fidelity entangled EPR pairs can be used to create remote entangled states of spin-squeezed type [3, 31, 32], possibly by following the approach for cat state preparation in remote optical cavities [33], or using local, collective interactions and repetitive teleportation [34–38]. In addition, while space-based communication networks will be capable of maintaining optical phase coherence for the links between clocks, we note that establishing ground-space coherent optical links remains a technical challenge and requires an intense research effort which has recently started [39]. Finally, if the entire network is spanned by satellites in space, the on-board local oscillators can further benefit from the much lower noise level compared to ground-based clocks.

If realized, such a quantum network of clocks can have important scientific, technological, and social consequences. Besides creating a world platform for time and frequency metrology, such a network may find important applications to a range of technological advances for earth science [41] and to the test and search for the fundamental laws of nature, including relativity and the connection between quantum and gravitational physics [42–45].

## SUPPLEMENTARY INFORMATION

### Appendix A: GHZ cascade in a network of $K$ clocks

Here, we discuss the details of using quantum correlated states constructed out of  $N' = Kn$  qubits, equally distributed among  $K$  clocks, namely the GHZ state of the form

$$[|00\dots 0\rangle + e^{i\chi}|11\dots 1\rangle]/\sqrt{2}, \quad (\text{A1})$$

where  $|qq\dots q\rangle = |q\rangle^{\otimes N'}$ ,  $q \in \{0, 1\}$ . Entanglement has two effects here: First, it makes the phase of such a GHZ state,  $\chi$ , sensitive to the accumulated phase of the *center-of-mass* of all the  $K$  independent local oscillators, (each located at one of the clocks)  $\Phi_{\text{LO}} = \sum_{j=1}^K \Phi^{(j)}/K$ , where  $\Phi^{(j)} = \int_0^T dt (\omega^{(j)}(t) - \omega_0)$  is the accumulated phase of the LO at clock  $j$ , during the interrogation time  $T$ , here  $\omega^{(j)}(t)$  is the instantaneous frequency of the LO, while  $\omega_0$  is the transition frequency of the clock qubit. Second, it

increases the sensitivity, due to quantum enhancement:

$$\begin{aligned} & \left( \prod_j^K \prod_i^{N'/K} \hat{U}_{i,j} \right) [|\mathbf{0}\rangle + e^{i\chi}|\mathbf{1}\rangle] / \sqrt{2} = \\ & = [|\mathbf{0}\rangle + e^{i(\chi + N'\Phi_{\text{COM}})}|\mathbf{1}\rangle] / \sqrt{2}, \quad (\text{A2}) \end{aligned}$$

where  $\hat{U}_{i,j} = |0\rangle\langle 0| + e^{i\Phi^{(j)}}|1\rangle\langle 1|$  is the time evolution operator during the interrogation time, acting on the  $i$ th qubit at clock  $j$ , and  $|\mathbf{0}\rangle$  and  $|\mathbf{1}\rangle$  are product states of all qubits being in  $|0\rangle$  or  $|1\rangle$ , respectively.

### 1. Parity measurement

By setting the initial phase of the GHZ state,  $\chi$ , to 0 and  $\pi/2$  in two parallel instances, we effectively measure the real and imaginary part of  $e^{iN'\Phi_{\text{COM}}}$ , and thus get an estimate on the value of  $N'\Phi_{\text{COM}}$  up to  $2\pi$  phase shifts. The most cost-effective way to do this is to measure all qubits in the local  $x$ -basis. In this basis, the state Eq. (A2) is written as

$$\frac{1}{\sqrt{2}} \left[ \left( \frac{|+\rangle - |-\rangle}{\sqrt{2}} \right)^{\otimes N'} + e^{i\phi} \left( \frac{|+\rangle + |-\rangle}{\sqrt{2}} \right)^{\otimes N'} \right], \quad (\text{A3})$$

where  $\phi = \chi + N'\Phi_{\text{COM}}$ , and  $|\pm\rangle = \frac{|0\rangle \pm |1\rangle}{\sqrt{2}}$ . The above state can be expanded in a sum:

$$\frac{1}{2^{(N'+1)/2}} \sum_{\mathbf{q} \in \{+, -\}^{\times N'}} \left[ \left( \prod_{j=1}^{N'} q_j \right) + e^{i\phi} \right] |q_1, q_2, \dots, q_{N'}\rangle, \quad (\text{A4})$$

where we labeled all qubits with  $k \in \{1, 2, \dots, N'\}$ , irrespective of which clock they belong to. The probability of a certain outcome  $\mathbf{q} = (q_1, q_2, \dots, q_{N'})$ , ( $q_j \in \{+, -\}$ ), is

$$\mathcal{P}(\mathbf{q}) = \frac{1}{2^{N'+1}} |1 + p(\mathbf{q})e^{i\phi}|^2, \quad (\text{A5})$$

where  $p(\mathbf{q}) = \prod_{j=1}^{N'} q_j$  is the parity of the sum of all measurement bits. Now, the clocks send their measurement bits to the center node, which evaluates  $p$ . This parity is the global observable that is sensitive to the accumulated phase, since its distribution is

$$\mathcal{P}(p = \pm) = \frac{1 \pm \cos(\phi)}{2}. \quad (\text{A6})$$

The above procedure is identical to the parity measurement scheme described in [14].

### 2. Cascaded GHZ scheme

Provided with  $N$  qubits distributed equally among  $K$  clocks, we imagine that each clock separates its qubits

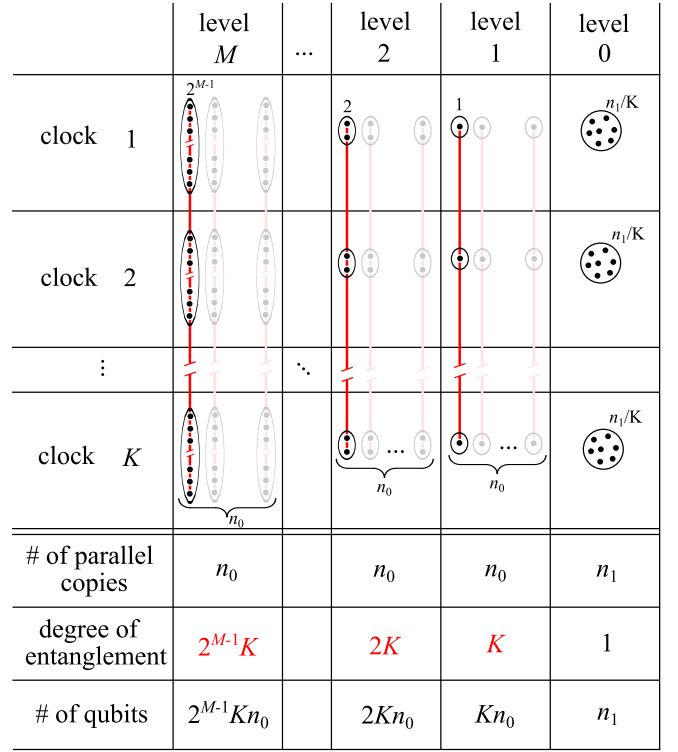


FIG. 5. GHZ cascade protocol for  $K$  clocks. Each allocates qubits for different levels of the protocol: In level 0,  $n_1/K$  qubits are put into an uncorrelated ensemble. In level  $i$ , ( $i = 1, 2, \dots, M$ ), each clock allocates  $n_0 2^{i-1}$  qubits for creating  $n_0$  parallel instances of GHZ states with  $2^{i-1}K$  entangled qubits. Due to the exponential scaling of the degree of entanglement, most of the total available qubits are used in higher levels of the cascade. This is a necessary condition to achieve Heisenberg scaling, up to logarithmic factors.

into  $M+1$  different groups. The 0th group contains  $n_1/K$  uncorrelated qubits, and the  $i$ th group ( $i = 1, 2, \dots, M$ ) contains  $n_0$  independent instances of  $2^{i-1}$  qubits that are entangled with the other groups of  $2^{i-1}$  qubits in each clock. In other words, there are  $n_0$  independent copies of GHZ states with a total of  $2^{i-1}K$  qubits entangled on the  $i$ th level of the cascade ( $i \geq 1$ ) (See Fig. 5). This way the total number of qubits can be written as

$$N = n_1 + n_0 \sum_{i=1}^M 2^{i-1}K \approx n_0 2^M K \quad (\text{A7})$$

where we assumed  $n_1 \ll N$ .

The purpose of this cascaded scheme is to directly assess the digits  $Y_1$  and  $\{Z_j : j = 2, 3, \dots\}$  in the binary fraction representation of the phase

$$\Phi_{\text{LO}} \bmod [-\pi, \pi] = \frac{2\pi}{K} \left[ Y_1 + \sum_{i=1}^{\infty} Z_{i+1}/2^i \right] - \pi, \quad (\text{A8})$$

where  $\bmod [-\pi, \pi] = (x + \pi) \bmod 2\pi - \pi$ ,  $Y_1 \in \{0, 1, 2, \dots, K-1\}$  and  $Z_i \in \{0, 1\}$ . The 0th level of the

cascade estimates  $\Phi_0 = \sum_{j=1}^K (\Phi^{(j)} \bmod [-\pi, \pi]) / K$ , and every  $i$ th level after that estimates  $\Phi_i = K2^{i-1}\Phi_{LO} \bmod [-\pi, \pi]$ . From these estimates one can determine the digits,

$$Y_1 = [K(\Phi_0 + \pi) - (\Phi_1 + \pi)] / (2\pi), \quad (\text{A9})$$

$$Z_i = [2(\Phi_{i-1} + \pi) - (\Phi_i + \pi)] / (2\pi), \quad (\text{A10})$$

for  $i = 2, 3, \dots, M$ .

The last group ( $i = M$ ) contains GHZ states with the most entangled qubits. These are the ones with the fastest evolving phase, and therefore they provide the best resolution on  $\Phi_{LO}$ . Since there are  $n_0$  independent instances, their phase  $\Phi_M = 2\pi \sum_{i=1}^{\infty} Z_{M+i}/2^i$  is known up to the uncertainty,  $\langle \Delta \Phi_M^2 \rangle_{\text{pr}} = \frac{1}{n_0}$ ,

Assuming that all lower digits  $\{Y_1, Z_j | j = 2 \dots M\}$  have been determined correctly, this results in the total measurement uncertainty for  $\Phi_{LO}$ :

$$\langle \Delta \Phi_{LO}^2 \rangle_{\text{pr}} = \frac{\langle \Delta \Phi_M^2 \rangle_{\text{pr}}}{(2^{M-1}K)^2} = \frac{4n_0}{N^2}, \quad (\text{A11})$$

where, for the moment, we neglected individual qubit noise and assumed  $\Phi_{LO} \in [-\pi, \pi]$ . However, in general, the estimation of the lower digits will not be perfect. In the following Section we investigate the effect of these *rounding errors* on the final measurement accuracy. From this analysis we find the optimal number of copies  $n_0$  and  $n_1$ .

### 3. Rounding errors

Whenever  $|\Phi_0^{\text{est}} - \Phi_0| > \pi/K$ , or  $|\Phi_i^{\text{est}} - \Phi_i| > \pi/2$  (for  $i \geq 1$ ), we make a mistake by under- or overestimating the number of phase slips  $Y_1$  or  $Z_{i+1}$ , respectively. To minimize the effect of this error, we need to optimize how the total of  $N$  qubits are distributed among the various levels of the cascade. In other words we need to find  $n_{0,\text{opt}}$  and  $n_{1,\text{opt}}$ .

The probability that a rounding error occurs during the estimation of  $Z_{i+1}$  is

$$\mathcal{P}_{i,\text{re}} = 2 \int_{\pi/D}^{\infty} d\phi \rho_i(\phi - \Phi_i) \leq 2 \int_{\pi/D}^{\infty} d\phi \frac{1}{s_i^3} \exp\left[-\frac{\phi^2}{2s_i^2}\right] \quad (\text{A12})$$

where  $\phi = \Phi_i^{\text{est}} - \Phi_i$ , and  $\rho_i$  is the conditional density function of  $\Phi_i^{\text{est}}$  for a given real  $\Phi_i$ , and  $s_i^2 = \text{Var}(\Phi_i^{\text{est}} - \Phi_i) = 1/n_0$  for  $i \geq 1$ , and  $s_0^2 = \langle \Delta \Phi_0^2 \rangle_{\text{pr}} = \frac{1}{K^2} \sum_{j=1}^K \langle (\Delta \Phi^{(j)})^2 \rangle_{\text{pr}} = 1/n_1$ , since  $\langle (\Delta \Phi^{(j)})^2 \rangle_{\text{pr}} = \frac{K}{n_1}$  for all  $j$ . The upper bound for  $\rho_i$  is obtained by using the following upper bound for any binomial distribution:  $\binom{m}{k} p^k (1-p)^{m-k} \leq \exp\left[-n \left(\frac{k}{n} - p\right)^2\right]$ . (For details, see Supplementary Materials of [12].) The resulting probabilities, after dropping the higher order terms in the

asymptotic expansions, are

$$\mathcal{P}_{0,\text{re}} \approx \frac{2K}{\pi} n_1^{1/2} \exp\left[-\frac{n_1 \pi^2}{2K^2}\right] \quad (\text{A13})$$

$$\mathcal{P}_{i,\text{re}} \approx \frac{4}{\pi} n_0^{1/2} \exp\left[-\frac{n_0 \pi^2}{8}\right] \quad (i \geq 1) \quad (\text{A14})$$

The phase shift imposed on the estimate of  $\Phi_{LO}$  by a manifested rounding error of  $Y_1$  is  $2\pi/K$  and of  $Z_i$  is  $2\pi/(K2^{i-1})$ , for  $i = 2, 3 \dots M$ . This results in the total variance contribution,

$$\langle \Delta \Phi_{LO}^2 \rangle_{\text{re}} = \left(\frac{2\pi}{K}\right)^2 \left[ \mathcal{P}_{0,\text{re}} + \sum_{i=2}^M \mathcal{P}_{i-1,\text{re}} (2^{-i+1})^2 \right] \quad (\text{A15})$$

$$\approx \left(\frac{2\pi}{K}\right)^2 \left[ \mathcal{P}_{0,\text{re}} + \frac{1}{3} \mathcal{P}_{i-1,\text{re}} \right]. \quad (\text{A16})$$

We simplify this expression by choosing  $n_1$  so that  $\mathcal{P}_{0,\text{re}} \approx \frac{2}{3} \mathcal{P}_{i,\text{re}}$ :

$$n_1 = \alpha K^2 n_0, \quad (\text{A17})$$

where  $\alpha \approx \max\left\{1, \frac{2}{\pi^2 n_0} \log\left(3K^2 \frac{\sqrt{8}}{\pi n_0^{1/2}}\right)\right\} \ll n_0, K$ .

With this choice, we can write the rounding error contribution as

$$\langle \Delta \Phi_{LO}^2 \rangle_{\text{re}} \approx \frac{16\pi}{K^2} n_0^{1/2} \exp\left[-\frac{n_0 \pi^2}{8}\right]. \quad (\text{A18})$$

We note that the amount of extra resources needed for the 0th level, is marginally small, since the total qubit number can be expressed as

$$N = n_1 + n_0 K \sum_{i=1}^M 2^{i-1} = n_0 K (\alpha K^2 + 2^M - 2) \approx n_0 K 2^M, \quad (\text{A19})$$

under the assumption  $K \ll 2^{M/2}$ .

By adding the two error contributions from Eq. (A11) and Eq. (A18), we obtain the corresponding Allan-variance,

$$\begin{aligned} \sigma_y^2(\tau) &= \frac{1}{\omega_0^2 \tau T} \langle \Delta \Phi_{LO}^2 \rangle =: \frac{1}{\omega_0^2 \tau} [\Gamma_1 + \Gamma_2] = \quad (\text{A20}) \\ &= \frac{1}{\omega_0^2 \tau} \left[ \frac{4n_0}{N^2 T} + \frac{16\pi}{K^2 T} n_0^{1/2} \exp\left[-\frac{n_0 \pi^2}{8}\right] \right] \quad (\text{A21}) \end{aligned}$$

Now, let us find the optimal value of  $n_0$ . We write  $\Gamma_1 + \Gamma_2$ , using the new variable  $x = \frac{8}{\pi^2} \frac{1}{n_0}$ , as

$$\Gamma_1 + \Gamma_2 = \frac{4}{T} \left( \frac{8}{\pi^2} \frac{1}{x N^2} + \frac{\sqrt{32}}{K^2} \frac{1}{x^{1/2}} \exp\left[-\frac{1}{x}\right] \right). \quad (\text{A22})$$

Taking the derivative with respect to  $x$  and equating it with 0, while using the assumption  $x \ll 1$  results in



$\Gamma_2 \approx x_{\text{opt}}\Gamma_1 \ll \Gamma_1$ , which can be written as the following transcendental equation for the optimal value,  $x_{\text{opt}}$ ,

$$x_{\text{opt}}^{1/2} \approx \frac{\pi^2 N^2}{\sqrt{8}K^2} \exp\left[-\frac{1}{x_{\text{opt}}}\right]. \quad (\text{A23})$$

The general solution of any equation of the form  $x^\nu = A \exp[-1/x]$ , in the limit of  $A \gg 1$  and  $x \ll 1$ , is  $x = [\log(A)]^{-1}$ . (For details, see the Supplementary Materials of [12].) Using this result we can write

$$x_{\text{opt}} \approx \left[\log\left(\frac{\pi^2 N^2}{\sqrt{8}K^2}\right)\right]^{-1} \sim [2\log(N/K)]^{-1} \quad (\text{A24})$$

$$n_{0,\text{opt}} \approx \frac{8}{\pi^2} \frac{1}{x_{\text{opt}}} \sim \left(\frac{4}{\pi}\right)^2 \log(N/K). \quad (\text{A25})$$

For the realistic case of  $N/K \gg 1$ , indeed  $x_{\text{opt}} \ll 1$ , and the corresponding minimal value of  $\Gamma_1 + \Gamma_2$  is

$$[\Gamma_1 + \Gamma_2]_{\min} \approx \Gamma_1(x_{\text{opt}}) = \left(\frac{8}{\pi}\right)^2 \frac{\log(N/K)}{N^2 T}. \quad (\text{A26})$$

This result indicates that, in terms of qubit number, only a logarithmic extra cost is required to achieve the Heisenberg limit.

#### 4. Phase slip errors

Although the cascade is designed to detect phase slips of all levels  $i = 1, 2, \dots, M$ , a possible phase wrap of level  $i = 0$  remains undetected. Since the qubits at different clocks are interrogated independently on the 0th level, each of them estimates the phase of the corresponding LO,  $\Phi_0^{(j)}$  ( $j = 1, 2, \dots, K$ ), and not  $\Phi_{\text{LO}}$ . The probability of  $\Phi_0^{(j)}$  falling outside the interval  $[-\pi, \pi]$  at least once during the total measurement time  $\tau$  is

$$\begin{aligned} \mathcal{P}_{j,\text{slip}} &= 2\frac{\tau}{T} \int_0^\infty d\phi \frac{1}{\sqrt{2\pi\gamma_{\text{LO}}T}} \exp\left[-\frac{\phi^2}{2\gamma_{\text{LO}}T}\right] \approx \\ &\approx \frac{\tau}{T} \frac{\sqrt{2}}{\pi^{3/2}} \sqrt{\gamma_{\text{LO}}T} \exp\left[-\frac{\pi^2}{2\gamma_{\text{LO}}T}\right], \end{aligned} \quad (\text{A27})$$

where  $\gamma_{\text{LO}}$  is the linewidth of the local oscillator at clock  $j$ , corresponding to a white noise spectrum, resulting in a constant phase diffusion over the interrogation time  $T$ , (which assumed to be approximately equal to the cycle time). The approximate form above is obtained by neglecting the higher order terms in the asymptotic series expansion under the assumption  $\gamma_{\text{LO}}T \ll 1$ . Once such a phase slip happens, it introduces a  $2\pi$  phase shift in  $\Phi_0^{(j)}$ , and therefore contributes to its overall uncertainty with  $\langle(\Delta\Phi_0^{(j)})^2\rangle = (2\pi)^2\mathcal{P}_{j,\text{slip}}$ . Physically  $\Phi_0$  is the phase of the COM signal, that the center can obtain after averaging the frequencies of all  $K$  local oscillators with equal weights,  $\Phi_0 = \Phi_{\text{COM}} = \sum_{j=1}^K \Phi_0^{(j)}/K$ , therefore  $\langle\Delta\Phi_0^2\rangle = \frac{1}{K^2} \sum_{j=1}^K \langle(\Delta\Phi_0^{(j)})^2\rangle = \frac{1}{K} \langle(\Delta\Phi_0^{(j)})^2\rangle$ , where

we assumed that the LOs are independent but they have the same linewidth,  $\gamma_{\text{LO}}$ . Since  $\Phi_0 = \Phi_{\text{LO}}$ , the above means the following variance contribution

$$\langle\Delta\Phi_{\text{LO}}^2\rangle_{\text{slip}} = \sqrt{32\pi} \frac{\tau\gamma_{\text{LO}}^{1/2}}{T^{1/2}K} \exp\left[-\frac{\pi^2}{2\gamma_{\text{LO}}T}\right]. \quad (\text{A28})$$

After adding this error to the previously minimized projection and rounding error terms (from Eq. (A26)), we obtain the corresponding Allan-variance,  $\sigma_y^2(\tau) = \frac{1}{\omega_0^2\tau} ([\Gamma_1 + \Gamma_2]_{\min} + \Gamma_3)$ , where

$$\begin{aligned} [\Gamma_1 + \Gamma_2]_{\min} + \Gamma_3 &= \\ &= \left(\frac{8}{\pi}\right)^2 \frac{\log(N/K)}{N^2} \frac{2\gamma_{\text{LO}}}{\pi^2} \frac{1}{y} + \frac{16}{\pi^{5/2}} \frac{\tau\gamma_{\text{LO}}^2}{K} \frac{1}{y^{3/2}} \exp\left[-\frac{1}{y}\right], \end{aligned} \quad (\text{A29})$$

using the variable  $y = \frac{2}{\pi^2}\gamma_{\text{LO}}T$ .

Now, let us find the optimal Ramsey time  $T_{\text{opt}}$ , under the assumption that  $\tau$  is sufficiently long. After taking the derivative with respect to  $y$  and equating it with zero, the assumption  $y_{\text{opt}} \ll 1$  results in the  $\Gamma_3 \approx y_{\text{opt}}[\Gamma_1 + \Gamma_2]_{\min} \ll [\Gamma_1 + \Gamma_2]_{\min}$  which can be written as the following transcendental equation,

$$y_{\text{opt}}^{3/2} \approx \frac{\pi^{3/2}}{8} \frac{\tau\gamma_{\text{LO}}}{K} \frac{N^2}{\log(N/K)} \exp\left[-\frac{1}{y}\right]. \quad (\text{A30})$$

The asymptotic solution in case of  $y_{\text{opt}} \ll 1$  is (see Supplementary of [12])

$$y_{\text{opt}} \approx \left[\log\left(\frac{\pi^{3/2}}{8} \frac{\tau\gamma_{\text{LO}}}{K} \frac{N^2}{\log(N/K)}\right)\right]^{-1}, \quad (\text{A31})$$

$$T_{\text{opt}} \approx \frac{\pi^2}{2} \frac{y_{\text{opt}}}{\gamma_{\text{LO}}} \sim \frac{\pi^2}{2\gamma_{\text{LO}}} [\log(\tau\gamma_{\text{LO}}N^2/K)]^{-1} \quad (\text{A32})$$

in the realistic limit of  $\gamma_{\text{LO}}\tau N^2/K \gg 1$ . The corresponding minimal Allan-variance is

$$\sigma_y^2(\tau) = \frac{1}{\omega_0^2\tau} \left([\Gamma_1 + \Gamma_2]_{\min} + \Gamma_3\right)_{\min} \approx \frac{1}{\omega_0^2} \frac{L\gamma_{\text{LO}}}{N^2\tau}, \quad (\text{A33})$$

where  $L = \frac{128}{\pi^4} \log(N/K) \log(\tau\gamma_{\text{LO}}N^2/K)$ .

For short  $\tau$  averaging times, the optimal Ramsey time is  $T_{\text{opt}} = \tau$ , instead of Eq. (A32). This makes  $\Gamma_3$  negligible compared to  $[\Gamma_1 + \Gamma_2]_{\min}$ , resulting in a  $1/\tau^2$  scaling:

$$\sigma_y^2(\tau) = \frac{1}{\omega_0^2\tau} [\Gamma_1 + \Gamma_2]_{\min}^{T=\tau} = \frac{1}{\omega_0^2} \frac{L'}{N^2\tau^2}. \quad (\text{A34})$$

where  $L' = \left(\frac{8}{\pi}\right)^2 \log(N/K)$ . This scaling is more favorable, but it continues to higher  $\tau$  values only up to  $\tau \sim \gamma_{\text{LO}}^{-1}$ , where it switches to the  $1/\tau$  behavior according to Eq. (A33).

#### 5. Pre-narrowing the linewidth

We can minimize the limiting effect of  $\gamma_{\text{LO}}$  by narrowing the effective linewidth of the local oscillators beforehand. We imagine using  $N^*$  qubits to locally pre-narrow

the linewidth of all LOs down to an effective linewidth  $\gamma_{\text{eff}} \sim \gamma_{\text{ind}}N$ , before using the rest  $N - N^*$  qubits in the GHZ cascade. This  $\gamma_{\text{eff}} \ll \gamma_{\text{LO}}$  allows the optimal Ramsey time going above the previous limit, set by  $\sim \gamma_{\text{LO}}^{-1}$  in Eq. (A32). This step-by-step linewidth narrowing procedure, using uncorrelated ensembles in every step, is outlined in [17, 18], and given detailed analysis in [12]. Working under the small  $N^*$  assumption, one can obtain  $\gamma_{\text{eff}}$  as

$$\gamma_{\text{eff}} \approx \gamma_{\text{LO}} \left[ \frac{2 \log(\gamma_{\text{LO}}\tau n)}{\pi^2 n} \right]^{N^*/n}, \quad (\text{A35})$$

where we imagine using  $n$  qubits in each narrowing step. We find the optimal value of  $n$  to be

$$n_{\text{opt}} \approx \frac{2e}{\pi^2} \log(\gamma_{\text{LO}}\tau), \quad (\text{A36})$$

by minimizing  $\gamma_{\text{eff}}$ , which yields

$$[\gamma_{\text{eff}}]_{\text{min}} \sim \gamma_{\text{LO}} \exp \left[ -\frac{N^*\pi^2}{2e \log(\gamma_{\text{LO}}\tau)} \right]. \quad (\text{A37})$$

For a given  $\tau$ , we can always imagine carrying out this pre-narrowing, so that  $\gamma_{\text{eff}} < \tau^{-1}$ , and therefore Eq. (A34) remains valid with the substitution  $N \mapsto N - N^*$  for  $\tau > \gamma_{\text{LO}}^{-1}$  as well. The required number of qubits,  $N^*$ , is

$$N^* \sim \frac{2e}{\pi^2} \log(\gamma_{\text{LO}}\tau) \log \left( \frac{\gamma_{\text{LO}}}{\gamma_{\text{ind}}N} \right) \ll N. \quad (\text{A38})$$

due to the exponential dependence in Eq. (A37).

## 6. Individual qubit dephasing noise

Our scheme, as well as any scheme, is eventually limited by individual qubit noise. Such a noise dephases GHZ states at an increased rate, compared to uncorrelated qubits, due to the entanglement, giving the corresponding variance contribution for the phase of the GHZ states in the  $M$ th group,  $\langle \Delta \Phi_M^2 \rangle_{\text{dephasing}} = \frac{2^{M-1}K\gamma_{\text{ind}}T}{n_0}$ , after averaging over the  $n_0$  independent copies of the GHZ states, each containing  $2^{M-1}K$  entangled qubits. The resulting variance contribution for  $\Phi_{\text{LO}}$  is

$$\langle \Delta \Phi_{\text{LO}}^2 \rangle_{\text{dephasing}} = \frac{\gamma_{\text{ind}}T}{n_0 2^{M-1}K} = \frac{2\gamma_{\text{ind}}T}{N}. \quad (\text{A39})$$

This term represents a noise floor, which we add to Eq. (A34) and obtain our final result for the minimal achievable Allan-variance,

$$\sigma_y^2(\tau) = \frac{1}{\omega_0^2} \left[ \frac{L'}{N^2\tau^2} + \frac{2\gamma_{\text{ind}}}{N\tau} \right]. \quad (\text{A40})$$

For long  $\tau$  times, the ultimate limit, set by the standard quantum limit,  $\sigma_y^2(\tau) = \frac{1}{\omega_0^2} \frac{\gamma_{\text{ind}}}{N\tau}$ , can be reached by

changing the base of the cascade. Instead of entangling 2-times as many qubits in each level of the cascade than in the previous level, we imagine changing it to a base number  $D$ . Carrying out the same calculation results in our final result for the achievable Allan-variance:

$$\sigma_y^2(\tau) = \frac{1}{\omega_0^2} \left[ \left( \frac{D}{2} \right)^2 \frac{L'}{N^2\tau^2} + \frac{D}{D-1} \frac{\gamma_{\text{ind}}}{N\tau} \right], \quad (\text{A41})$$

where  $L' = \left( \frac{8}{\pi} \right)^2 \log(N/K)$ . (See Supplementary of [12] for details.) The optimal value of  $D$  depends on  $\tau$ . For small  $\tau$ ,  $D_{\text{opt}} = 2$ , however for large  $\tau$  one can gain a factor of 2 by choosing  $D_{\text{opt}} = D_{\text{max}}$ . Due to natural constraints,  $D_{\text{max}} \sim \sqrt{N}$ , in which regime, the protocol consists of only two cascade levels, an uncorrelated 0th level, with  $\sim \sqrt{N}$  qubits and an entangled 1st level with  $\sim N$  qubits.

## Appendix B: Security countermeasures

### 1. Sabotage

In order to detect sabotage, the center can occasionally perform assessment tests of the different nodes by teleporting an uncorrelated qubit state  $[|0\rangle + e^{i\chi}|1\rangle]/\sqrt{2}$ , where  $\chi$  is a randomly chosen phase known only to the center. A properly operating node creates a local GHZ state  $[|\mathbf{0}\rangle + e^{i\chi}|\mathbf{1}\rangle]/\sqrt{2}$  from the sent qubit, measures the parity of the GHZ state, and sends it to the center. The measured parity holds information on the phase  $\phi' = \chi + \phi$ , where  $\phi$  is the accumulated phase of the LO at the node. Due to the random shift  $\chi$ , this appears to be random to the node, and therefore indistinguishable from the result of a regular (non-testing) cycle. On the other hand, the center can subtract  $\chi$ , and recover  $\phi$  from the same measurement results. In the last step, the center verifies  $\phi$  by comparing it with the classically determined phase  $\phi_{\text{cl}}$  of the sent LO signal with respect to the COM signal. The expected statistical deviation of  $\phi$  from  $\phi_{\text{cl}}$  is  $\Delta(\phi - \phi_{\text{cl}}) \sim \sqrt{\frac{K}{N}}$ , while the accuracy of the COM phase  $\Delta(\phi_{\text{COM}} - T\omega_0) \sim \sqrt{\frac{K}{(K-K_t)N}}$  is much smaller, where  $K_t$  is the number of simultaneously tested nodes. In the likely case of  $K_t \ll K$ , this method is precise enough for the center to discriminate between healthy and unhealthy nodes by setting a acceptance range,  $|\phi - \phi_{\text{cl}}| \leq \Lambda \sqrt{\frac{K}{N}}$ . E.g. the choice of  $\Lambda = 4$  results in a “4 $\sigma$  confidence level”, meaning only 0.0063% chance for false positives (healthy node detected as unhealthy), and similarly small chance for false negatives (unhealthy node being undetected) ( $\sim \Lambda \frac{\Delta\phi'}{2\pi} \propto 1/\sqrt{N}$ ) due to the high precision with which  $\phi'$  is measured. The fact, that the teleported qubit can be measured only once, also prevents the nodes from discovering that it is being tested.

## 2. Eavesdropping

Eavesdroppers would try to intercept the sent LO signals, and synthesize the stabilized  $\nu_{\text{COM}}$  for themselves. Our protocol minimizes the attainable information of this strategy by prescribing that only the *non-stabilized* LO signals are sent through classical channels. This requires the feedback to be applied to the LO signal after some of it has been split off by a beam splitter, and the center to integrate the generated feedback in time. Alternatively, eavesdroppers could try intercepting the LO signals *and* the feedback signals, and gain access to the same information, the center has. This can be prevented by encoding the radio frequency feedback signal with phase modulation according to a shared secret key. Since such a key can be shared securely with quantum key distribution, this protocol keeps the feedback signal hidden from outsiders. As a result, even the hardest-working eavesdropper, who intercepts all LO signals, is able to access only the non-stabilized COM signal, and the stabilized COM signal remains accessible exclusively to parties involved in the collaboration.

## 3. Rotating center role

Since the center works as a hub for all information, ensuring its security has the highest priority. In a scenario, where none of the nodes can be trusted enough to play the permanent role of the center, a rotating stage scheme can be used. By passing the role of the center around, the potential vulnerability of the network due to one untrustworthy site is substantially lowered. This requires a fully connected network and a global scheme for assigning the role of the center.

## Appendix C: Network operation

### 1. Different degree of feedback

Apart from the full feedback, described in the main text, alternatively, the center can be operated to provide restricted feedback information to the nodes. If the center sends the averaged error signal  $\tilde{\delta}_{\text{COM}}$  only, the LOs at the nodes will not benefit from the enhanced stability and only the center can access the stabilized signal. Of course the LO at each node will have its own local feedback to keep it within a reasonable frequency range around the clock transition. Such a 'safe' operational mode makes the center node the only participant having access to the world time signal.

As an intermediate possibility, the center can choose to send regionally averaged feedback signals  $\tilde{\delta}_{\text{COM}} + \sum_{j \in R} (\nu_j - \nu_{\text{COM}})/|R|$ , uniformly for all  $j \in R$  nodes, where  $R$  is a set of nodes, ie. a region. Such a feedback scheme creates the incentive of cooperation for the nodes in region  $R$ . By properly sharing their LO signals with

each other, the nodes can synthesize the regional COM frequency,  $\sum_{j \in R} (\nu_j)/|R|$ , and steer it with the feedback, received from the center.

### 2. Timing

Proper timing of local qubit operations is necessary to ensure that every qubit in the network is subject to the same  $T$  free evolution time. The finite propagation time of light signals introduces delays in the quantum links and classical channels. Similarly, during the entangling step, the finite time required to do CNOT operations make the free evolution start at slightly different times for different qubits. Since both the initialization and the measurement are local operations, we can resolve the issue of delay by prescribing that the measurement of qubit  $i_j$  ( $i$ th qubit at node  $j$ ) takes place exactly  $T$  time after its initialization. Occasional waiting times of known length can be echoed out with a  $\pi$ -pulse at half time.

In extreme cases, this might cause some qubits to be measured before others are initialized. However, this is not a problem, since the portion of the GHZ state that is alive during the time in question is constantly accumulating the  $\phi_j$  phases from the qubits it consists of. This results in the phenomenon that the total time of phase accumulation can be much longer than the length of individual phase accumulations, provided that the said interrogations overlap.

### 3. More general architectures

So far, we focused on the simplest network structure with one center initiating every Ramsey cycle and nodes with equal number of clock qubits.

In a more general setup, node  $j$  has  $N_j$  clock qubits. If  $N_j$  is different for different  $j$ , then the nodes will contribute the the global GHZ states unequally, resulting in entangled states which consists of different  $N'_j$  number of qubits from each site  $j$ . Such a state picks up the phase

$$\Phi = \sum_j N'_j \phi_j, \quad (\text{C1})$$

where  $\phi_j$  is the phase of the LO at site  $j$  relative to the atomic frequency. As a result, the clock network measures the following collective LO frequency

$$\nu_{\text{LO}} = \frac{\sum_j N'_j \nu_j}{\sum_j N'_j}. \quad (\text{C2})$$

This represents only a different definition of the world time (a weighted average of the times at the locations of the nodes, instead of a uniform average), but it does not affect the overall stability.

The initial laser linewidths of the nodes  $\gamma_{\text{LO}}^j$  can also be different. The stability achievable in this case is

bounded by the stability obtained for a uniform linewidth  $\gamma_{\text{LO}} = \max_j \gamma_{\text{LO}}^j$ . If linewidths are known, the center can divide the best estimation method which uses linewidth dependent weights in the LO frequency averaging step.

Although it is simple to demonstrate the important network operational concepts with the architecture with one center, this structure is not a necessary. The quantum channels, connecting different nodes, can form a sparse (but still connected) graph, and the entanglement global entanglement can still be achieved by intermedi-

ate nodes acting as repeater stations. This way entanglement can be passed along by these intermediate nodes. Moreover, the center can be eliminated from the entangling procedure by making the nodes generate local GHZ states, and connect them with their neighbors by both measuring their shared EPR qubit with one of the qubits form the local GHZ state in the Bell-basis. After communicating the measurement result via classical channels, and performing the required single qubit operations, a global GHZ state is formed.

- 
- [1] Nicholson, T. L. *et al.* Comparison of Two Independent Sr Optical Clocks with  $1 \times 10^{-17}$  Stability at  $10^3$  s. *Physical Review Letters* **109**, 230801 (2012).
- [2] Hinkley, N. *et al.* An atomic clock with  $10^{-18}$  instability. *Science* **341**, 1215–1218 (2013).
- [3] Leroux, I. D., Schleier-Smith, M. H. & Vuletić, V. Implementation of Cavity Squeezing of a Collective Atomic Spin. *Physical Review Letters* **104**, 073602 (2010).
- [4] Ye, J. *et al.* Delivery of high-stability optical and microwave frequency standards over an optical fiber network. *J. Opt. Soc. Am. B* **20**, 1459 (2003).
- [5] Droste, S. *et al.* Optical-Frequency Transfer over a Single-Span 1840km Fiber Link. *Physical Review Letters* **111**, 110801 (2013).
- [6] Cirac, J., Zoller, P., Kimble, H. & Mabuchi, H. Quantum State Transfer and Entanglement Distribution among Distant Nodes in a Quantum Network. *Physical Review Letters* **78**, 3221–3224 (1997).
- [7] Kimble, H. J. The quantum internet. *Nature* **453**, 1023–1030 (2008).
- [8] Perseguers, S., Lapeyre, G. J., Cavalcanti, D., Lewenstein, M. & Acín, A. Distribution of entanglement in large-scale quantum networks. *Reports on progress in physics. Physical Society* **76**, 096001 (2013).
- [9] Nielsen, M. A. & Chuang, I. L. *Quantum Computation and Quantum Information* (Cambridge University Press, Cambridge, 2000).
- [10] Duan, L. M., Lukin, M. D., Cirac, J. I. & Zoller, P. Long-distance quantum communication with atomic ensembles and linear optics. *Nature* **414**, 413–418 (2001).
- [11] Wineland, D. *et al.* Experimental issues in coherent quantum-state manipulation of trapped atomic ions. *Journal of Research of the National Institute of Standards and Technology* **103**, 259 (1998).
- [12] Kessler, E. M. *et al.* to be published.
- [13] Giedke, G., Taylor, J., DAlessandro, D., Lukin, M. & Imamolu, A. Quantum measurement of a mesoscopic spin ensemble. *Physical Review A* **74**, 032316 (2006).
- [14] Bollinger, J., Itano, W., Wineland, D. & Heinzen, D. Optimal frequency measurements with maximally correlated states. *Physical Review A* **54**, R4649–R4652 (1996).
- [15] Leibfried, D. *et al.* Toward Heisenberg-limited spectroscopy with multiparticle entangled states. *Science* **304**, 1476–1478 (2004).
- [16] With different number of qubits at each node, the weighted average needs to be taken.
- [17] Rosenband, T. & Leibbrandt, D. R. Exponential scaling of clock stability with atom number (2013). arXiv:1303.6357.
- [18] Borregaard, J. & Sørensen, A. S. Efficient Atomic Clocks Operated with Several Atomic Ensembles. *Physical Review Letters* **111**, 090802 (2013).
- [19] Escher, B. M., de Matos Filho, R. L. & Davidovich, L. General framework for estimating the ultimate precision limit in noisy quantum-enhanced metrology. *Nature Physics* **7**, 406–411 (2011).
- [20] Borregaard, J. & Sørensen, A. S. Near-Heisenberg-Limited Atomic Clocks in the Presence of Decoherence. *Physical Review Letters* **111**, 090801 (2013).
- [21] Gisin, N., Ribordy, G., Tittel, W. & Zbinden, H. Quantum cryptography. *Reviews of Modern Physics* **74**, 145–195 (2002).
- [22] Chou, C. W., Hume, D. B., Koelemeij, J. C. J., Wineland, D. J. & Rosenband, T. Frequency Comparison of Two High-Accuracy  $\text{Al}^{+}$  Optical Clocks. *Physical Review Letters* **104**, 070802 (2010).
- [23] Cirac, J. & Zoller, P. A scalable quantum computer with ions in an array of microtraps. *Nature* **404**, 579–581 (2000).
- [24] Monz, T. *et al.* 14-Qubit Entanglement: Creation and Coherence. *Physical Review Letters* **106**, 130506 (2011).
- [25] Olmschenk, S. *et al.* Quantum teleportation between distant matter qubits. *Science* **323**, 486–489 (2009).
- [26] Chou, C.-W. *et al.* Functional quantum nodes for entanglement distribution over scalable quantum networks. *Science* **316**, 1316–1320 (2007).
- [27] Togan, E. *et al.* Quantum entanglement between an optical photon and a solid-state spin qubit. *Nature* **466**, 730–734 (2010).
- [28] Bernien, H. *et al.* Heralded entanglement between solid-state qubits separated by three metres. *Nature* **497**, 86–90 (2013).
- [29] Risté, D. *et al.* Deterministic entanglement of superconducting qubits by parity measurement and feedback (2013). arXiv:1306.4002.
- [30] Dür, W., Briegel, H.-J., Cirac, J. & Zoller, P. Quantum repeaters based on entanglement purification. *Physical Review A* **59**, 169–181 (1999).
- [31] Sherson, J. F. *et al.* Quantum teleportation between light and matter. *Nature* **443**, 557–560 (2006).
- [32] Ma, X.-S. *et al.* Quantum teleportation over 143 kilometres using active feed-forward. *Nature* **489**, 269–273 (2012).
- [33] Haroche, S. & Raimond, J.-M. *Exploring the Quantum: Atoms, Cavities, and Photons* (Oxford University Press, USA, 2006).
- [34] Jia, X. *et al.* Experimental Demonstration of Unconditional Entanglement Swapping for Continuous Variables.

- Physical Review Letters* **93**, 250503 (2004).
- [35] Kessler, E. M. *et al.* in preparation.
- [36] Takei, N. *et al.* Experimental demonstration of quantum teleportation of a squeezed state. *Physical Review A* **72**, 042304 (2005).
- [37] Lee, N. *et al.* Teleportation of nonclassical wave packets of light. *Science* **332**, 330–333 (2011).
- [38] Andersen, U. L. & Ralph, T. C. High Fidelity Teleportation of Continuous Variable Quantum States using Delocalized Single Photons (2013). arXiv:1302.1359.
- [39] Djerroud, K. *et al.* Coherent optical link through the turbulent atmosphere. *Optics letters* **35**, 1479–1481 (2010).
- [40] Maunz, P. *et al.* Quantum interference of photon pairs from two remote trapped atomic ions. *Nature Physics* **3**, 538–541 (2007).
- [41] Tapley, B. *et al.* GGM02 – An improved Earth gravity field model from GRACE. *Journal of Geodesy* **79**, 467–478 (2005).
- [42] Abramovici, A. *et al.* LIGO: The Laser Interferometer Gravitational-Wave Observatory. *Science* **256**, 325–333 (1992).
- [43] Seidel, A. *et al.* The ACES Microwave Link: Instrument Design and Test Results. In *2007 IEEE International Frequency Control Symposium Joint with the 21st European Frequency and Time Forum*, 1295–1298 (IEEE, 2007).
- [44] Schiller, S. *et al.* Einstein Gravity Explorer a medium-class fundamental physics mission. *Experimental Astronomy* **23**, 573–610 (2008).
- [45] Wolf, P. *et al.* Quantum physics exploring gravity in the outer solar system: the SAGAS project. *Experimental Astronomy* **23**, 651–687 (2008).

#### ACKNOWLEDGEMENT

We are grateful to Till Rosenband and Vladan Vuletić for enlightening discussions. This work was supported by NSF, CUA, ITAMP, HQOC, JILA PFC, NIST, DARPA QUSAR, the Alfred P. Sloan Foundation, the Quiness programs, ARO MURI, and the ERC grant QIOS (grant no. 306576); MB acknowledges support from NDSEG and NSF GRFP. It is dedicated to Rainer Blatt and Peter Zoller on the occasion of their 60th birthday, when initial ideas for this work were formed.

#### COMPETING FINANCIAL INTERESTS

The authors declare no competing financial interests.